Communication Scheduling to Minimize Thermal Effects of Implanted Biosensor Networks in Homogeneous Tissue

Qinghui Tang, Naveen Tummala, Sandeep K. S. Gupta, *Senior Member, IEEE,* and Loren Schwiebert *Senior Member, IEEE,*

***Abstract*— A network of biosensors can be implanted in a human body for health monitoring, diagnostics, or as a prosthetic device. Biosensors can be organized into clusters where most of the communication takes place within the clusters, and long range transmissions to the base station are performed by the cluster leader to reduce the energy cost. In some applications, the tissues are sensitive to temperature increase and may be damaged by the heat resulting from normal operations and the recharging of sensor nodes. Our work is the first to consider rotating the cluster leadership to minimize the heating effects on human tissues. We explore the factors that lead to temperature increase, and the process for calculating the Specific Absorption Rate (SAR) and temperature increase of implanted biosensors by using the Finite-Difference Time-Domain (FDTD) method. We improve performance by rotating the cluster leader based on the leadership history and the sensor locations. We propose a simplified scheme, Temperature Increase Potential, to efficiently predict the temperature increase in tissues surrounding implanted sensors. Finally, a genetic algorithm is proposed to exploit the search for an optimal temperature increase sequence.**

***Index Terms*— Specific Absorption Rate, Bioheating, FDTD, Genetic Algorithms, Scheduling, Clustering, Wireless Sensor Networks.**

I. Introduction

A BIOSENSOR is a device that detects, records, and transmits information regarding a physiological change in its environment. Data transfer for an implanted biosensor must use wireless communication as it is impractical to distribute wires throughout the body. A group of biosensors can form a system [1] for continuous monitoring of oxygen on the surface of exteriorized tissues, or to form an electrode sensor array used for a retina prosthesis [2]. We envision a future where sensors can form a wireless sensor network comprising a large number of nodes whose placement in the body can be either pre-determined or random according to the application [3].

Since biosensors must operate with very limited power, energy efficiency is an important aspect in designing such applications. Prior research shows that a cluster-based communication protocol (CB) is more energy efficient than a tree-based approach [4]. CB is based on the idea that energy consumption can be reduced by having only a small fraction of nodes perform long range communication with a base station. These nodes are called cluster leaders. All the non-leader nodes register themselves with one of these cluster leaders.

The cluster leader collects information from all the nodes in its cluster and forwards this information to a base station. Thus, it expends energy at a higher rate than other nodes and the leadership role must be rotated to average communication power consumption over all sensor nodes and to extend network lifetime. However, no previous work has been done on rotating leadership to minimize the heating effects of implanted sensor networks.

Radiation from wireless communication and power dissipation of an implanted sensor will heat the surrounding tissues. For example, radio frequency (RF) waves used in wireless communication produce electrical and magnetic fields. Human tissue will absorb heat and experience a temperature increase when exposed to electromagnetic fields. Our research group is conducting research on implanted biosensors used as a retina or cortical prosthesis [2], so our concerns over minimizing the heat absorption and the temperature increase caused by implanted sensors motivates this work.

For safety reasons, the level of radiation being absorbed by the human body needs to be measured. Specific Absorption Rate (SAR) is measured in units of W/kg and records the rate at which radiation energy is absorbed by tissue per unit weight. The relationship between radiation and SAR is given by

$$SAR = \frac{\sigma |E|^2}{\rho} \ (W/kg)\,, \tag{1}$$

where E is the induced electric field, ρ is the density of the tissue, and σ is the electrical conductivity of the tissue. Many countries and organizations set strict standards for peak SAR. Experiments show exposure to an SAR of 8W/kg in any gram of tissue in the head or torso for 15 minutes may have a significant risk of tissue damage [6]. Even with more modest heating, organs that are especially sensitive to any temperature increase due to a lack of blood flow to them are prone to thermal damage (e.g., lens cataracts [7]). Researchers have also expressed concern about the heating of the eye by examining the SAR and the temperature of the eye when exposed to a Wireless LAN [8] or Infrared [9] radiation.

In our study, we demonstrate that selection of the next leader should not be random, as has been done in other cluster based protocols, since random selection may result in a higher temperature increase in surrounding tissues. Our contributions in this paper are:

- **Modeling thermal effects of implanted biosensors.** Using a radiation model based on RF powering and the properties of the communication antenna, and a power dissipation model for the sensor circuitry, we use the Finite-Difference Time-Domain (FDTD) method to calculate the SAR and the temperature increase in homogeneous tissue.
- **Identifying factors that minimize thermal effects of a cluster-based implanted sensor network**. We show the necessity of leader rotation, and the importance of considering the leadership history and the sensor locations to lower temperature increase and to prevent potential thermal hazards to the tissue.
- **Development of the Temperature Increase Potential (TIP) and a Genetic Algorithm (GA) for fast computation of a minimal temperature increase rotation sequence.**

In Section II, we give an overview of related work. We describe our system model in Section III. We discuss the calculation of SAR and temperature increase in Section IV. We explore the necessity and importance of the leader rotation sequence in Section V. We then introduce the Temperature Increase Potential algorithm in Section VI. In Section VII, we discuss optimized sequence searching algorithms by using our genetic algorithm and compare its results with other approaches through simulation.

This work is supported in part by NSF grants ANI-00196156, ANI-0086020 and ANI-0123980.

Qinghui Tang, Naveen Tummala, and Sandeep Gupta are with the Department of Computer Science and Engineering, Arizona State University at Tempe, AZ. 85287 USA. E-mail: {qinghui.tang, naveen.tummala, sandeep.gupta}@asu.edu.

Loren Schwiebert is with the Department of Computer Science, Wayne State University at Detroit, MI. 48202. E-mail: loren@wayne.edu.

II. Related Work

Although sensors have been around for a long time, recent technological revolutions have greatly enhanced their application in medicine, which has led to much research in related areas. Even though there has been a considerable amount of research done in wireless ad-hoc communication protocols, these results are not feasible for wireless biosensor networks as most of them have not taken into account the dangers of tissue heating due to the power dissipation of sensors.

Gosalia *et al.* [10] conducted experiments and analysis on measuring the thermal elevation in the vitreous cavity and retina due to implanted electronics. This work considers only one heating source and focuses on measuring temperature increase, whereas we assume a group of sensors working as heating sources and we propose to use scheduling to reduce temperature increase. In addition, it assumes an external radiation source but we model an implanted radiation source since this is the actual scenario. In our analysis, the tissue experiences a smaller temperature increase due to the rotation of the leader node, while in [10] a much higher temperature increase was observed due to the contiguous heating from the implanted electronics and the larger power dissipation.

A great deal of research has been done on radiation absorption and heating effects on the human body. Moneda *et al.* [11] investigate radio frequency wave absorption on a human head model. Hirata *et al.* [7] calculate the SAR for the interaction of the human eye with electromagnetic waves in the Industrial, Scientific, and Medical (ISM) frequency bands. They evaluate the possible health hazards especially for the human eye, such as microwave induced cataract formation, with various electromagnetic waves throughout the human body. This work partially motivates our investigation into the potential hazards to the eye caused by the temperature increase of implanted biosensor networks. Bernardi *et al.* [8] evaluate the temperature increase in the human eye due to radiation from a Wireless LAN. Riu and Foster [12] conduct a numerical study on the SAR produced by microwave radiation from a half-wavelength dipole using a near tissue model. Both papers consider only one of the two radiation sources, namely, RF powering or wireless communication.

Heinzelman *et al.* propose a Low Energy Adaptive Clustering Hierarchy protocol (LEACH) [5], a clustering protocol that uses random rotation of local cluster heads to evenly distribute the energy consumption among the sensors in the network. The LEACH protocol selects the next leader based on a probability function that favors nodes with more energy. The disadvantage of such an approach is that the next selected node is possibly near the previous leader, resulting in repeatedly heating the same tissue. In our solution, the next sensor leader is selected based on sensor location and rotation history.

III. System Model

A. Cluster-based Networking and Rotation of the Cluster Leader

A smart biosensor node contains one or several sensors, a processor, and a transceiver combined on a chip. A small group of sensor nodes form a cluster. There may be several clusters in the network. We consider the heating of tissue within a specific small area, which is called the ***control volume***; see Fig. 1. We assume all sensors inside a control volume are the members of a single cluster. The base station is assumed to know the exact location of these sensors. This is reasonable since sensors are assumed to be surgically implanted and monitored after implantation for precise location. The cluster leader collects information from all the non-leader nodes and transmits it to the base station. The leader node will be charged with all the other nodes in the cluster because the omnidirectional propagation of RF waves prevents it from being focused on only a single sensor node.

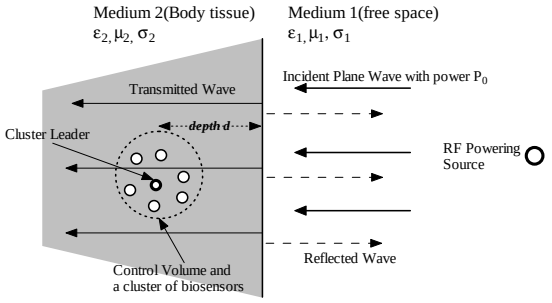

Fig. 1. System Model: A cluster of implanted sensors.

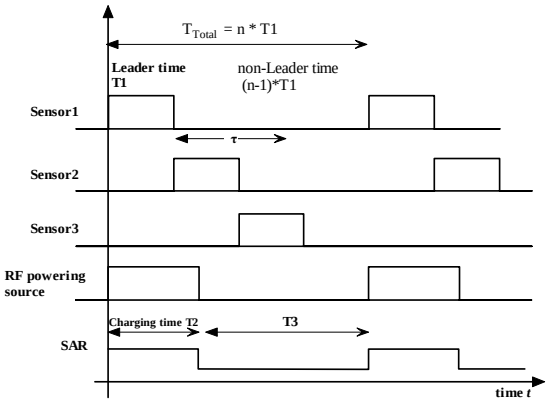

Fig. 2. Working period of sensors, cluster leader is rotated every T_1 units of time.

The working period of the leader is shown in Fig. 2. The cluster leadership has to be rotated every T_1 units of time. The reason for rotating the cluster leader is the additional heating of the tissue surrounding the leader due to the power dissipation of the sensor and the tissue's exposure to RF waves. Rotation also provides the previous leader with a cooling down period. The next leader is selected after T_1 units of time. The sequence of cluster leadership can be predetermined or selected on the fly. The base station choose the next leader based on the state of nodes, such as the locations, the leadership history, the energy reserves, and the local temperatures. After every T_3 time period, all sensors are recharged for a T_2 time period. During the recharging period, the SAR rises due to the radiation from RF inductive powering. Otherwise, the SAR has a relatively small value consisting of the communication radiation of sensor nodes.

The smart biosensor nodes are rechargeable, i.e., that the network has a renewable power supply. There are several possible power sources that can be used for sensor nodes, such as infrared (IR) radiation, solar power, and mechanical energy derived from vibrations. However, these approaches are all still preliminary without mature applications. Another available and mature power source is RF powering [13], including magnetic-coupling based inductive link [14] and electronic-coupling based passive E-field [15]. This has the ability to charge many sensors simultaneously. Thus, RF powering is the most practical power source for implanted biosensor applications.

B. Temperature Measurement

The temperature surrounding the sensor nodes can be measured by using a temperature sensor inside the sensor node's circuitry, but this will raise the cost and increase the complexity of sensor circuit. So in our model we assume that we cannot measure the temperature surrounding the sensor node. The rate of temperature

increase depends on the characteristics of the human body such as perfusion rate, specific conductivity, and metabolic heating.

C. Problem Statement

Our problem is that given a control volume, the known locations of implanted sensors, and the related properties, how to schedule the rotation sequence to reach a minimum temperature increase and to minimize the heat effects on the tissue.

IV. Using FDTD to Calculate Temperature Increase

A. Heating of tissue

We identify three major sources of heating of tissues:

1) ***Heating caused by RF Powering****:* The sensor nodes are recharged by an external RF power source. The frequency ω of the RF power supply is normally between 2 MHz and 20 MHz [16] [17]. The power absorbed by the tissue surrounding the sensor is one of the main sources of tissue heating. The propagation of RF waves can be simulated as a plane wave. As shown in Fig. 1, on the boundary between the air (medium 1, characterized by conductivity σ_1, relative permittivity ϵ_1, and permeability μ_1) and the human body (medium 2, characterized by σ_2, ϵ_2, and μ_2), part of the wave is reflected and the rest is transmitted into medium 2. The relationship between incident power density W_0 and transmitted power density W_t is given by [18]

$$W_t = \left(1\text{-}\left|\Gamma\right|^2\right) W_0,\ \Gamma = \frac{\eta_2 - \eta_1}{\eta_2 + \eta_1},\ \eta_i = \frac{\sqrt{\mu_i/\varepsilon_i}}{\sqrt{1 - \frac{\sigma_i}{j\omega\varepsilon_i}}}, \quad (2)$$

where $i = 1$ or 2, Γ is the reflection coefficient, and η_i is the intrinsic impedance. The power density of the incident wave degrades exponentially as it penetrates into the human body and at a depth d (in meters) we have [18]

$$W_d = W_t e^{-2\alpha d} = \left(1 - \left|\Gamma\right|^2\right) W_0 e^{-2\alpha d}\ (W/m^2), \quad (3)$$

where the attenuation constant α is:

$$\alpha = \omega\sqrt{\frac{\mu\epsilon}{2}}\left[\sqrt{1 + \left(\frac{\sigma}{\omega\epsilon}\right)^2} - 1\right]^{1/2} (Neper/m). \quad (4)$$

Since the relationship between the incident electrical field $|E|^2$ and power density is

$$W_d = \frac{1}{2}\,\mathrm{Re}\left\{\frac{1}{\eta}\right\}|E|^2_{RF}\ (W/m^2), \quad (5)$$

we can calculate the SAR due to the radiation from RF powering as

$$SAR_{RF} = \frac{\sigma\,|E|^2_{RF}}{\rho} = \frac{2\sigma W_d}{\rho\,\mathrm{Re}\left\{\frac{1}{\eta}\right\}}\ (W/kg). \quad (6)$$

2) ***Radiation from the Sensor Node's Antenna****:* Sensor nodes use wireless communication to exchange data among themselves. Radiation from a wireless antenna is another heating factor that needs to be examined carefully. We assume that the sensor node has a short dipole antenna consisting of a short conducting wire of length dl, terminated in two small conductive spheres or disks. Assume that the current I is uniform and varies sinusoidally with time. To analyze the effects of radiation on the tissue, we assume the tissue to be homogeneous with no sharp edges and rough surfaces. The space around the antenna is divided into the near field and the far field. The region of space immediately surrounding the antenna is known as the near field. The extent of the near field is given by $d_0 = \frac{\lambda}{2\pi}$, where λ is the RF wavelength for wireless communication. SAR in the near and the far field are given by [19] and [20], respectively:

$$SAR_{NF} = \frac{\sigma\mu\omega}{\rho\sqrt{\sigma^2 + \epsilon^2\omega^2}}\left(\frac{Idl\sin\theta e^{-\alpha R}}{4\pi}\left(\frac{1}{R^2} + \frac{|\gamma|}{R}\right)\right)^2, \quad (7)$$

$$SAR_{FF} = \frac{\sigma}{\rho}\left(\frac{\alpha^2 + \beta^2}{\sqrt{\sigma^2 + \omega^2\epsilon^2}}\frac{Idl}{4\pi}\right)^2 \frac{\sin^2\theta e^{-2\alpha R}}{R^2}, \quad (8)$$

where R is the distance from the source to the observation point, θ is the angle between the observation point and the xy plane, and γ is the propagation constant.

We assume our 2D control volume is located in the xy plane and it is perpendicular to the small dipole, thus we can safely assume the radiation pattern is omnidirectional on the 2D plane and $\sin\theta = 1$. The near field and the far field radiation of the sensor's transmitter cause heating of the tissue because of the absorption of the radiation. Combining (3), (7), and (8), the total SAR is

$$SAR_{all} = \begin{cases} SAR_{RF} + SAR_{NF} & \text{for} \quad R \leqslant \frac{\lambda}{2\pi} \\ SAR_{RF} + SAR_{FF} & \text{for} \quad R > \frac{\lambda}{2\pi} \end{cases}, \quad (9)$$

3) ***Power Dissipation by the Sensor Node Circuitry****:* The power dissipation of the sensor circuitry will raise the temperature of sensor nodes. The power consumed by the sensor circuitry divided by the volume of sensor, is the power dissipation density, denoted as P_c, which depends on its implementation technology and architecture. In our analysis, we have considered the typical power consumption for regular sensor circuit operation.

B. Calculating Temperature Increase

The above mentioned sources of heating can cause a temperature increase inside the control volume. The rate of this increase in temperature is given by the Pennes bioheat equation [21] as follows

$$\rho C_p\frac{dT}{dt} = K\bigtriangledown^2 T - b(T - T_b) + \rho SAR + P_c + Q_m\ (W/m^2), \quad (10)$$

where ρ is the mass density, C_p is the specific heat of the tissue, K is the thermal conductivity of the tissue, b is the blood perfusion constant, which indicates how fast the heat can be taken away by the blood flow inside the tissue, and T_b is the temperature of the blood and the tissue. $\frac{dT}{dt}$ is the rate of temperature increase in the control volume. Terms on the right side indicate the heat accumulated inside the tissue. The terms $K\bigtriangledown^2 T$ and $b(T - T_b)$ are the heat transfer due to the thermal conduction and the blood perfusion, respectively. The terms ρSAR, P_c, and Q_m are the heat generated due to radiation, the power dissipation of circuitry, and the metabolic heating, respectively.

FDTD [22] is an electromagnetic modeling technique that discretizes the differential form of time and space, which can be used in a heating application. The entire problem space is discretized into small cells that are marked with a pair of coordinates (i, j). For space reasons, we show only the result of the new bioheat equation after some discretization manipulations

$$\begin{aligned} T^{m+1}(i,j) = {} & \left[1 - \frac{\delta_t b}{\rho C_p} - \frac{4\delta_t K}{\rho C_p\delta^2}\right] T^m(i,j) \\ & + \frac{\delta_t}{C_p}SAR + \frac{\delta_t b}{\rho C_p}T_b + \frac{\delta}{\rho C_p}P_c \\ & + \frac{\delta_t K}{\rho C_p\delta^2}\left[\begin{array}{l} T^m(i+1,j) + T^m(i,j+1) \\ +T^m(i-1,j) + T^m(i,j-1) \end{array}\right], \end{aligned} \quad (11)$$

where $T^{m+1}(i,j)$ is the temperature of cell (i,j) at time $m+1$, δ_t is discretized time step, and δ is the discretized space step.

From (11), we can find the temperature of cell point (i,j) at time $m+1$, which is a function of the temperature at cell point (i,j) at time m, as well as a function of the temperature of surrounding cell points $((i+1,j)$, $(i,j+1)$, $(i-1,j)$, and $(i,j-1))$ at time m. Using Eq. (9) and Eq. (11), we can compute the distribution of the SAR and the temperature increase inside the control volume.

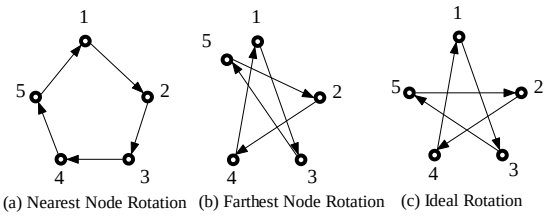

Fig. 3. Five Node Cluster

V. Impact of Leadership History and Sensor Location

A. Leadership Rotation Sequences

In determining the next leader, the following two factors are significant: the location of the next leader and the leadership history. For example, consider the simple cluster of five sensor nodes depicted in Fig. 3(a) and a rotation sequence, 1→2→3→4→5, which we denote as the Nearest Node Rotation (NNR) sequence. After node 1 completes its leadership tenure, node 2 takes over the leadership and performs the long range transmission. At this point, the tissue between sensor node 1 and sensor node 2 is heated continuously, and the temperature rises to a relatively high level.

And for Farthest Node Rotation (FNR), we select the next leader based on its Euclidean distance from the current leader. So the rotation sequence is 1→3→5→2→4 (see Fig. 3(b)). In this case, node 1 is the first leader followed by node 3. Since node 1 has already been the leader, even though it is the farthest one from node 3, it will not be considered. Thus, as the second farthest node from node 3, node 5 will be the next leader. But node 5 is not the ideal node to be a leader because of its proximity to node 1 and the presence of residual heat from node 1's leadership.

Now consider the scenario with sequence 1→3→5→2→4, which has an evenly distributed location (see Fig. 3(c)). We call this the Ideal Node Rotation (INR) sequence. By comparing the temperature increase results of the NNR sequence, FNR sequence, and INR sequence, we will find out whether the leader rotation history and the sensor locations have an influence on the temperature increase.

B. Simulation Setup

We use the tissue properties and wave propagation characteristics shown in Table I. We assume our control volume is homogeneously composed of muscle. Values for the dielectric properties are obtained from the Federal Communications Commission (FCC) [23], and the tissue related properties are obtained from [24] . We have not considered the metabolic heat generation in the simulation because its effect on the overall temperature increase is negligible.

The power consumption of a typical implanted sensor used for a retina prosthesis ranges from 11mW to 60mW [24], depending on the voltage and current of the power source. In other research work, the power consumption of a passive telemetry IC [25] is 0.5mW. So in our simulation, we assume the power consumption of a cluster leader is 5mW and a non-leader sensor consumes 1mW. The frequencies used for RF powering and wireless communication are set to 2MHz and 2.45GHz [24], respectively. We assume the non-leaders use about one-tenth the power used by the leader node for communication. Initially, temperatures of all the sensors and the tissue are set to a normal human body temperature of $37^{\circ}C$. The control volume is divided into 30×30 cells.

An improper resolution for the cell size and the time step can cause the FDTD fail to converge. As a rule of thumb, the shortest guided wavelength of interest should be at least 10 to 20 times the cell size. In our case, the shortest wavelength is $0.122m$, so we chose $0.005m$ as our cell size. If the cell size is smaller than $0.005m$, the calculation time and the memory used increases exponentially with the size and no significant difference is gained from the simulation. Also, $0.005m$ is a reasonable size for a small implanted sensor, since we assume each sensor occupies an entire cell.

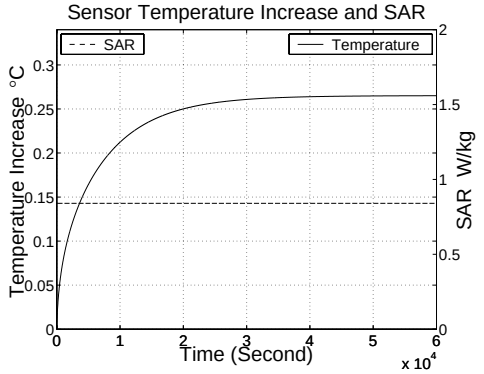

Fig. 4. Static Leader.

To ensure the stability of the solver of Eq. (11), we need

$$1 \geqslant \frac{\delta_t b}{\rho C_p} + \frac{4\delta_t K}{\rho C_p \delta^2}, \text{ or } \delta_t \leqslant \frac{1}{\frac{b}{\rho C_p} + \frac{4K}{\rho C_p \delta^2}} = 40.976. \qquad (12)$$

To get a better approximation of the resulting figure, we chose $10s$ as our time step.

C. Simulation Results

*1) **Static Leader**:* In this scenario, there is no leader rotation among the sensors. The tissue surrounding the leader is heated continuously due to the circuitry power consumption and the communication radiation. The heat conduction rate and the convection rate caused by blood perfusion also increase with the tissue temperature. In our simulation, the tissue temperature reaches steady state after 30000 seconds. As shown in Fig. 4(a), the temperature increase reaches $0.265^{\circ}C$ in steady state. The SAR is a constant of $0.8402W/kg$ because of the fixed radiation from the static leader. Although the temperature increase and the SAR seem relatively small, in an environment with higher radiation and critical application requirements, such a rise can be hazardous to the tissue.

Similar results of the same order are also observed in the experiment of Gosalia *et al.* [10] ($0.82^{\circ}C$ for implanted chip position) and the numerical analysis of Lazzi *et al.* [26] ($0.6^{\circ}C$ in the eye and $0.2^{\circ}C$ in the retina). In our simulation, however, the tissue experiences a smaller and slower temperature increase due to the relatively weak heating source applied in our analysis (in [10], power dissipation is assumed between 12.4mW and 49.6mW) and the different tissue properties.

*2) **Comparison of INR, NNR, and FNR**:* Fig. 5 shows the temperature increase and the SAR of node 5 when using NNR, FNR, and INR. When the sensor is heated by the power dissipated by itself or by the radiation of its neighbors, it experiences a rise in the SAR. Temperature begins to rise when the SAR is high and temperature drops when the SAR is low.

In Fig. 5(a), the INR sequence is 1→3→5→2→4. When node 1 is the leader, node 5 is heated slightly because it is near node 1. When node 2 is the leader, node 5 has one period leadership time to cool down. During node 5's leadership time, the SAR is as high as 0.83W/kg and the peak temperature is $0.212^{\circ}C$. After that, node 5 has two periods of leadership time to cool down. The smallest temperature increase of node 5 is $0.174^{\circ}C$.

In Fig. 5(b), NNR has the sequence 1→2→3→4→5. Since the leadership of each cluster node is passed to its neighbor, each node

TABLE I
PARAMETERS AND THEIR VALUES USED IN SIMULATION

Parameter	Property	value	Parameter	Property	value
ε_r	Relative permittivity at 2MHz or 2.45GHz	826 or 52.73	σ	Conductivity at 2MHz or 2.45GHz	0.5476 or 1.7388 $\left[\frac{S}{m}\right]$
P_{NL}	Power consumption of non-leader sensor node	$1mW$	P_L	Power consumption of Leader node	5 mW
C_p	Specific heat	3600 $\left[\frac{J}{kg^\circ C}\right]$	T_1	Leader Time	600 sec
K	Thermal conductivity	0.498 $\left[\frac{J}{ms^\circ C}\right]$	δ	Control Volume cell size	0.005 m
b	Blood perfusion constant	2700 $\left[\frac{J}{m^3 s^\circ C}\right]$	δ_t	Time step of FDTD	10 sec
T_b	Fixed blood temperature	37 $^\circ C$	T_2	Charging time	600 sec
P_0	Power Density of incident plane wave	10 $\left[\frac{W}{m^2}\right]$	I_0	Current provided to sensor node antenna	0.1 A
ρ	Mass density	1040 $\frac{kg}{m^3}$			

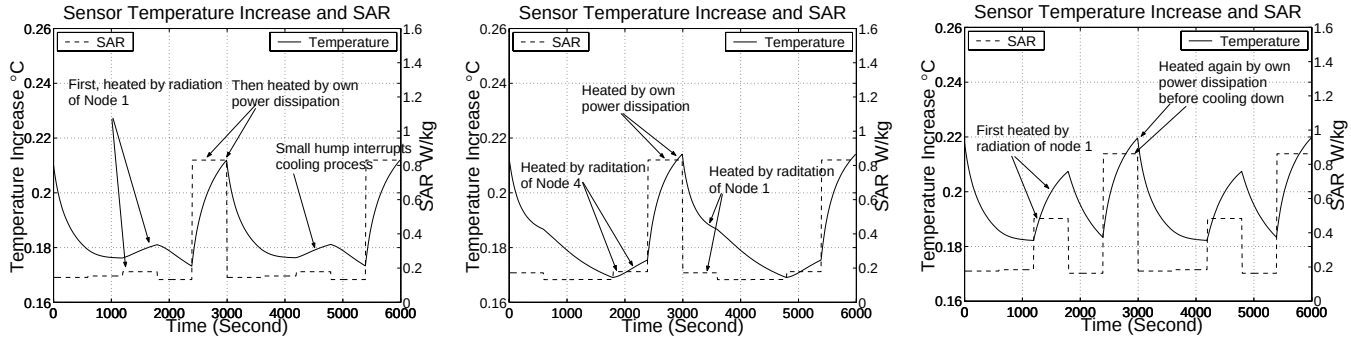

(a) Ideal Rotation Sequence of Fig 3(a) with Peak Value $0.212^\circ C$ and Lowest Value $0.174^\circ C$.

(b) Nearest Node Rotation Sequence of Fig 3(b) with Peak Value $0.215^\circ C$ and Lowest Value $0.169^\circ C$.

(c) Farthest Rotation Sequence of Fig 3(c) with Peak Value $0.22^\circ C$ and Lowest Value $0.184^\circ C$.

Fig. 5. Temperature Increase and SAR of sensor node 5 under Ideal Rotation, Nearest Node Rotation and Farthest Node Rotation

is heated consecutively by its preceding leader node, itself, and the succeeding leader node. The highest temperature increase of node 5 is $0.215^\circ C$, a little higher than that of Ideal Rotation.

In Fig. 5(c), FNR has the sequence 1→3→5→2→4. During node 1's leadership tenure, node 5 experiences a sharp increase in SAR and temperature due to its adjacency to node 1, whereas in Fig. 5(a) and Fig. 5(b), small SARs caused by neighbors lead to only small temperature increases. After node 3's leadership tenure, node 5 is selected as the next leader, which disrupts the cooling time of node 5, causing the SAR value and the temperature of node 5 to rise again. Thus, the peak temperature increase is $0.22^\circ C$ for node 5, which is much higher than the maximum temperature increase using the Ideal Rotation approach. Due to node 1's influence, the heat of node 5 cannot dissipate effectively.

*3) **Simulation Conclusion**:* Obviously, different rotation sequences result in different temperature increases and the leadership history and the sensor locations should be considered in selecting the next leader. Improper sequence may lead to dangerously high temperature. The problem of leader selection and rotation is to find a leader rotation sequence with the peak temperature that will not exceed a safety limit. The sequence with lowest temperature increase is the optimal solution.

VI. SIMPLIFIED TEMPERATURE INCREASE PREDICTION SCHEME

It takes about 2 minutes to test each sequence with our FDTD simulation program, which is running on a Pentium 4 desktop with a 2.4GHz CPU and 1GB memory. We estimate that it would take more than 720,960 hours to test all sequences if we have a ten-sensor cluster which has total $P_{10}^{10} = 10!$ possible sequences. To improve the efficiency of testing a sequence, we propose a simplified scheme to estimate the possible temperature increase of each sequence.

A. Time-Space Function

Given a single node that operates periodically as the leader, the temperature increase of any other node inside the control volume depends on both the Euclidean distance from the leader node, d, and the time τ, which is the time elapsed since the leader's previous leadership tenure, as show in the working period of sensor 1 in Fig. 2. Obviously, the larger the values of d and τ, the smaller the temperature increase is, and vice versa.

We denote this relationship as the time-space function $f(\tau, d)$, which depends on a time-variant heating source and has no closed form expression. But given the settings in Table I, we can obtain the numeric value of $f(\tau, d)$ using FDTD, as shown with the mesh lines in Fig. 6. The x-axis shows the change due to the distance in millimeters. The y-axis shows the change due to the elapsed time in terms of T_1, the length of the leadership interval.

Using the nonlinear surface fitting of Table Curve 3D [27] and the Minimum Mean Square Error (MMSE) criteria, we get the fitting function of $f(\tau, d)$ as

$$g(\tau, d) = \frac{1}{c_1 + c_2 d^{0.5} + c_3 \tau^2 + c_4 \tau^{2.5} + c_5 \tau^3}, \qquad (13)$$

with the values of the coefficients are: c_1 = 14.8827, c_2 = 8.8633, $c_3 = 3.1134$, c_4 = -1.5933, c_5 = 0.2471.

The numerical values of $g(\tau, d)$ are shown as dots in Fig. 6. As can be observed, the surface fitting function $g(x, y)$ does not perfectly match the distribution of function $f(x, y)$. The standard deviation of

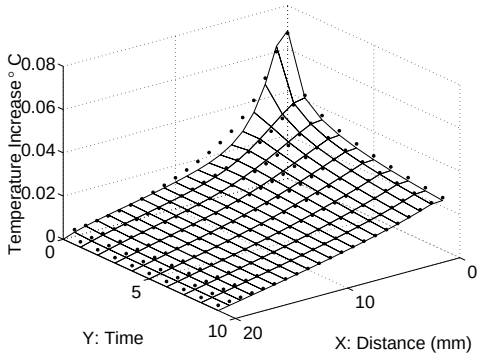

Fig. 6. Time-Space function. X-axis: distance from the heating source (leader node). Y-axis: time elapsed since the previous leader tenure.

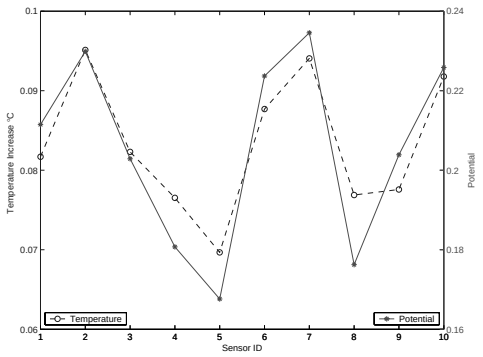

Fig. 7. Temperature Increase Potential (TIP) predicts the trend of temperature increase. High TIP results in high temperature increase, or vice versa.

the estimation error is within $0.0004^{\circ}C$. With such a small estimation error, it is reasonable for us to use $g(\cdot)$ to estimate the temperature increase and to find the near-optimal sequence with TIP, as discussed in Section VII.

When several nodes have approximately the same temperature increase, the estimation error could result in the actual highest temperature increase node being incorrectly estimated as having the second or third highest temperature increase. In such cases, we can assume all such nodes share the same peak temperature increase.

B. Rotation Distance and Location Distance

Each pair of sensor nodes, e.g., node i and node j, has different positions inside the rotation sequence, which is denoted by **rotation distance** c_{ij}. The physical explanation of rotation distance is the time elapsed between the leadership tenures of node i and node j. Obviously, a smaller rotation distance c_{ij} indicates node j will have a higher temperature increase, because after being heated by node i, node j soon becomes leader and further heats this surrounding tissue.

Notice that c_{ij} may not be the same value as c_{ji}. For example, in sequence (5 2 8 6 1 7 3 4 10 9), the positions of node 2 and node 8 are second and third, respectively. In this example, c_{28}, the rotation distance between node 2 and node 8, is $(3-2)=1$; but c_{82}, the rotation distance between node 8 and node 2, is $(2-3) \mod 10 = 9$.

Each pair of nodes, e.g., node i and node j, has a fixed Euclidean distance between them. We denote this distance as **location distance** L_{ij}. A smaller Euclidean distance L_{ij} indicates that node i has more influence on the temperature increase of node j because of a shorter distance between the two nodes.

C. Potential

Now we summarize the relationship between the temperature increase of a node, and its rotation distance and location distance. We denote P_{ij} as ***Temperature Increase Potential*** (TIP), which is the influence of node i's leadership on the temperature increase of node j and is a function of L_{ij} and c_{ij}. Observing the time-space function $f(\tau, d)$, we notice the physical meaning of L_{ij} is the same as d, and similarly, c_{ij} is the same as τ. Thus, we can define TIP as

$$P_{ij} = f(c_{ij}, L_{ij}) \approx g(c_{ij}, L_{ij}). \tag{14}$$

The joint influence on one node is the sum of the individual influences from all other heating sources, so we have

$$P_j = \sum_{i=1}^{N} P_{ij} \approx \sum_{i=1}^{N} g(c_{ij}, L_{ij}). \tag{15}$$

Since $g(\tau, d)$ is an approximation of the possible temperature increase, we can use TIP to estimate the possible temperature increase, but not to calculate the exact temperature increase value. Prediction errors may occur due to approximation error, so we need verify its effectiveness.

D. Verification of Temperature Increase Potential (TIP) Calculations

We perform tests to verify TIP's effectiveness in predicting which node will have the peak temperature increase. We focus on a cluster with ten randomly distributed sensors. We calculate TIP with 500 random locations and random rotation sequences, and use the FDTD simulation program to obtain the peak temperature increase for these same scenarios, then compare the TIP results with the temperature increase for these various scenarios.

Fig. 7 shows one of the simulation results that compares the actual temperature increases and TIPs of the sensors. As can be seen, although TIPs are not the exact values of the temperature increase, they have the same trend. That is, a node that has a high TIP will have a high temperature increase. Similarly, a node that has a low TIP value will have a low temperature increase.

We also want to determine how accurately TIP can predict which node has the highest temperature increase. Statistics from the 500 simulation runs show that the prediction is correct about 90.6% of the time. In another 8.2% of the cases, the node with the predicted highest temperature increase is actually the node with the second or the third highest temperature increase. This happens due to the approximation error of TIP as previously mentioned, and also due to the small difference between the node with the highest temperature increase, and the second or third highest. Our simulation statistics show that when an error occurs, the maximal temperature difference amongst the highest two (three) temperature increases is about $0.0015^{\circ}C$. With such a small variation, we can assume all these nodes have the same peak temperature increase. Taking into account close cases like this, TIP can correctly predict which node has the highest temperature increase in 98.8% of the instances.

E. Optimal Sequence and Worst Sequence

We enumerate and test all possible sequences of 10 sensors and find the optimal sequence and the worst sequence. The optimal sequence with the lowest peak potential is (5 7 1 6 10 8 4 2 9 3), whose peak potential is 0.2336 and its peak temperature increase is $0.0934^{\circ}C$, which is experienced by node 2. The mean temperature increase for node 2 is $0.829^{\circ}C$, and the standard deviation is $0.0062^{\circ}C$. The worst sequence is (5 4 3 8 1 6 9 10 2 7), whose peak potential is 0.248. It has a peak temperature increase of $0.1051^{\circ}C$ (experienced by node 7), a mean of $0.0840^{\circ}C$, and a standard deviation of $0.0117^{\circ}C$.

Fig. 8 compares the performance in terms of the peak value, the mean (in the form of an errorbar), and the standard deviation of

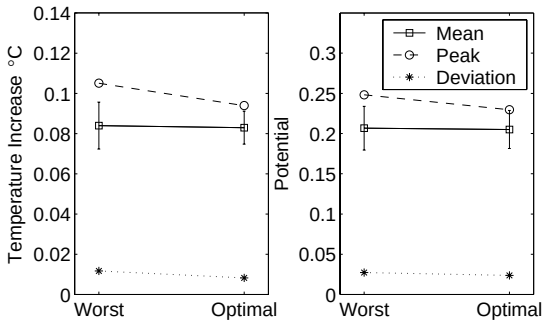

Fig. 8. Comparison of the optimal sequence and the worst sequence.

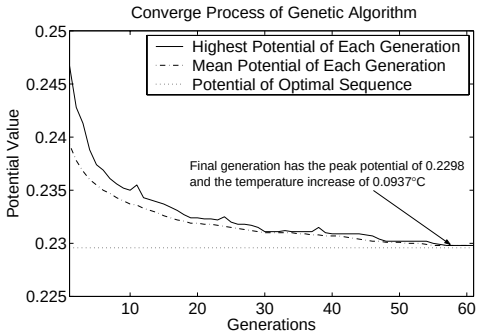

Fig. 9. Results of the genetic algorithm for each generation.

the optimal sequence and the worst sequence. We can see that as the performance becomes better (peak value becomes lower), the standard deviation becomes smaller, which means the heat absorption and temperature increase is more equally distributed across all ten sensors. Even though the mean stays unchanged or decreases only a little, the peak temperature increase continuously decreases. Also, comparing Fig. 8(a) and Fig. 8(b), we can observe that the TIP demonstrates the same trend of performance change as the real temperature. Thus, TIP is a reliable estimate of the real temperature increase.

VII. Finding Near-Optimal Sequence Using GA

The problem of finding an efficient rotation sequence is somewhat similar to the well-known Traveling Salesman Problem (TSP), which is an NP-complete problem. Note that the metric between two cities in the TSP is static, whereas for our problem the temperature increase depends on leadership history and hence the metric is dynamic.

For a small number of sensors, it is easy to find a good rotation sequence by observation or by enumeration For a cluster with many sensors, enumeration would be a laborious procedure. In certain applications, the near-optimal solution exhibits performance similar to optimal solutions and satisfies the application requirements. And searching a near-optimal solution greatly reduces the time and cost of seeking an optimal solution.

In the following we will show how to use a Genetic Algorithm (GA) optimization approach to find a near-optimal rotation sequence. GA is a stochastic optimization algorithm that simulates the processes of evolution in nature [28]: mutation and survival of the fittest.

A. Sequence Selection Process

1) ***Evolutionary Process****:* The chromosome of each individual is the rotation sequence. The temperature increase or TIP of each individual is used as the fitness measure. An individual with a lower temperature increase is healthier and more likely to survive the selection process.

Initially, we establish a random pool of possible solutions with various sequences. In each generation, new individuals (new sequences) are created by mating existing individuals (the crossover process) and mutation. Then new individuals and preexisting individuals experience the selection process together. Sequences with higher fitness enter into the next round of the evolutionary process with higher probability, and begin another round of mating, mutation, and selection. The evolutionary process continues until new sequences do not show a significant improvement in fitness compared with their parents. The best individuals in the last generation are near-optimal solutions.

2) ***Crossover Process****:* We use the Order Crossover proposed by Davis [29]. During the process, pairs of individuals are randomly selected and mate with each other. Randomly selected segments of the chromosomes are swapped to generate two new individuals (new sequences) in the next generation.

3) ***Mutation Process****:* We randomly select one individual with very low probability (since the probability of mutation in nature is extremely low, too), and randomly select two positions of its sequence, then swap the two numbers for a new sequence. For example, we have (1 2 3 4 5 6 7 8 9), and the mutation transposes the 4th and 7th positions. We end up with a new mutated sequence as follows: (1 2 3 4 5 6 7 8 9) -> (1 2 3 7 5 6 4 8 9).

4) ***Selection Process****:* All the individuals and the newly generated children are combined for the Roulette Wheel selection process [28]. The individuals with a higher fitness will have a higher probability to be selected and survive in this selection round. They are also qualified for further generation selection processes. At the same time, individuals with poor fitness are usually eliminated. Sequences with lower temperature increase are prone to survive and mate with other excellent sequences to get even more promising sequences.

B. Simulation Results for the Genetic Algorithm

We use the TIP to accelerate the estimation of fitness of each individual population and use (15) as our objective function. Each generation has 50 sequences. The mutation probability is 0.1%. The generation gap, the number of new children compared with that of the parent population, is 40%. The insertion rate, the percentage of top fittest individuals to replace the least fit parents, is 50%. We run the simulation for 60 generations, since more generations shows no further improvement in the final result.

The results of the evolutionary process are shown in Fig. 9. Initially, the potentials of the first generation are distributed in a wide range, with a peak value of 0.2467 and a mean of 0.2393. As the selection process continue, the highest potential and the mean potential of each generation gradually decrease. The mean potential of all nodes gradually decreases from 0.2393 to 0.2298, indicating that the distribution of heat absorption becomes more even.

Finally, all the individuals converge to the same sequence and have the same potential value. The final generation of the genetic algorithm has the sequence (5 7 9 3 10 8 4 2 6 1) with a peak potential of 0.2298, which is very close to the potential of the optimal sequence: 0.2296. We test this sequence with FDTD and the result shows this sequence has a peak temperature increase of $0.0937^{\circ}C$, which is very close to the temperature increase of the optimal sequence: $0.0934^{\circ}C$.

The time used by the four different approaches are shown in Table II. FDTD plus GA take about 100 hours to test a total of 3000 sequences. TIP plus GA take just 5 minutes. Combining TIP with GA significantly shorten the time for finding an near-optimal solution that has a performance very close to the optimal sequence.

In Fig. 10, we compare the distributions of temperature increase for three different sequences. Notice that from left to right, the

TABLE II
TIME EFFICIENCY OF FOUR DIFFERENT SEQUENCE FINDING APPROACHES

Approaches	Solution	Time Used
FDTD & enumeration	Optimal	720960 hours (estimated)
FDTD & GA	Near-optimal	100 hours (estimated)
TIP & enumeration	Optimal	7.6 hours
TIP & GA	Near-optimal	5 minutes

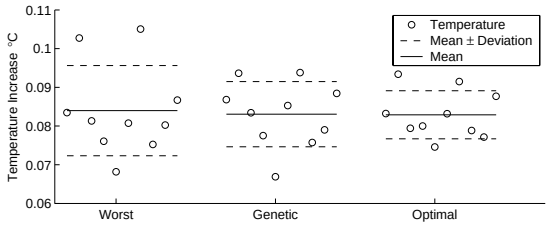

Fig. 10. Comparison of Temperature Distribution of Different Sequences: as standard deviation decreases, distribution density increases and temperature increase becomes more evenly distributed.

distribution density of sensor temperature increase gradually rises, and the peak temperature increases and its standard deviation gradually decreases. Again, this verifies our observation that a good scheduling rotation sequence has a low temperature increase and smaller standard deviation, which means the heat absorption is more equally distributed across all sensors and the thermal effects are minimized.

VIII. CONCLUSIONS AND FUTURE WORK

In this paper, we report our study on the heating problem for implanted biosensor networks. Previous research showed rotation of the cluster leader is necessary to distribute energy consumption equally across all sensors. For biomedical applications, however, the tissue may be sensitive to the temperature increase, so considering energy consumption is not enough. We explore the factors that need to be considered to calculate temperature increase and the Specific Absorption Rate for sensor nodes. Specifically, we define Temperature Increase Potential (TIP) as an efficient way to speed up the estimation of the temperature increase. We show by using a genetic algorithm combined with TIP that we can find near-optimal solutions much faster than enumerating sequences and testing them with FDTD. In future work, we plan to expand our model into a three-dimensional heterogeneous one, which is a more practical model of the human body. We will also analyze the heating effects with consideration of the effects of energy efficient channel coding and wireless link budget analysis.

REFERENCES

[1] B. J. Sargent and D. A. Gough, "Design and validation of the transparent oxygen sensor array," *IEEE Tran. Biomedical Eng.*, vol. 38, no. 5, pp. 476–482, May 1991.

[2] L. Schwiebert, S. K. S. Gupta, P. S. G. Auner, G. Abrams, R. Lezzi, and P. McAllister, "A biomedical smart sensor for visually impaired," in *IEEE Sensors 2002*, Orlando, FL., USA, June 2002.

[3] A. Salhieh, J. Weinmann, M. Kochhal, and L. Schwiebert, "Power efficient topologies for wireless sensor networks," in *Proceedings of the 2001 International Conference on Parallel Processing*. IEEE Computer Society, 2001, pp. 156–166.

[4] V. Shankar, A. Natarajan, S. K. S. Gupta, and L. Schwiebert, "Energy-efficient protocols for wireless communication in biosensor networks," in *Proc. of 12th IEEE Int'l Symp. Personal, Indoor and Mobile Radio Comm.*, San Diego, USA, Sept. 2001, pp. D–114–D–118.

[5] W. R. Heinzelman, A. Chandrakasan, and H. Balakrishnan, "Energy-efficient communication protocol for wireless microsensor networks," in *Proceedings of the 33rd Hawaii International Conference on System Sciences-Volume 8*. IEEE Computer Society, 2000, p. 8020.

[6] "Medical electrical equipment, part 2-33: Particular requirement for the safety of magnetic resonance systems for medical diagnosis IEC 60601-2-33," International Electrotechnical Commission IEC.

[7] A. Hirata, G. Ushio, and T. Shiozawa, "Calculation of temperature rises in the human eye for exposure to EM waves in the ISM frequency bands," in *IEICE Trans. Comm.*, vol. E83-B, no. 3, 2000, pp. 541–548.

[8] P. Bernardi, M. Cavagnaro, S. Pisa, and E. Piuzzi, "SAR distribution and temperature increase in an anatomical model of the human eye exposed to the field radiated by the user antenna in a wireless LAN," *IEEE Trans. Microwav Theory Tech.*, vol. 46, no. 12, pp. 2074–2082, Dec. 1998.

[9] J. A. Scott, "The computation of temperature rises in the human eye induced by infrared radiation," *Phys. Med. Biol.*, vol. 33, no. 2, pp. 243–257, 1988.

[10] K. Gosalia, J. Weiland, M. Humayun, and G. Lazzi, "Thermal elevation in the human eye and head due to the operation of a retinal prosthesis," *IEEE Tran. Biomedical Eng.*, vol. 51, no. 8, pp. 1469–1477, Aug. 2004.

[11] A. P. Moneda, M. P. Ioannidou, and D. P. Chrissoulidis, "Radio-wave exposure of the human head: Analytical study based on a versatile eccentric spheres model including a brain core and a pair of eyeballs," *IEEE Trans. Biomedical Eng.*, vol. 50, no. 6, pp. 667–676, 2003.

[12] P. J. Riu and K. R. Foster, "Heating of tissue by near-field exposure to a dipole: A model analysis," *IEEE Tran. Biomedical Eng.*, vol. 46, no. 8, pp. 911–917, 1999.

[13] P. R. Troyk and M. A. K. Schwan, "Closed-loop class E transcutaneous power and data link for microimplants," *IEEE Tran. Biomedical Eng.*, vol. 39, no. 6, pp. 589–599, June 1992.

[14] P. A. Neukomm, "Passive telemetry by absorption modulation, a new principle for long-term transabdominal monitoring of pressure and EMG of the uterus of a cow," in *Proc. 10th Int'l Symp. on Biotelemetry*, Fayetteville, USA, 1988, pp. 487–496.

[15] D. N. P. A. Neukomm, I. Roncoroni and H. H. Quick, "Passive e-field telemetry: A new wireless transmission principle in minimally invasive medicine," in *Proc. 15th Int'l Symp. on Biotelemetry*, May 1999.

[16] W. J. Heetderks, "RF powering of millimeter and submillimeter-sized neural prosthetic implants," *IEEE Tran. Biomedical Eng.*, vol. 35, no. 5, pp. 323–327, May 1988.

[17] W. Mokwa and U. Schnakenberg, "Micro transponder systems for medical applications," *IEEE Tran. Instrumentation and Measurements*, vol. 50, no. 6, pp. 1551–1555, Dec. 2001.

[18] F. T. Ulaby, *Fundamentals of Applied Electromagnetics*. Prentice-Hall, 1999.

[19] Y. Prakash, S. Lalwani, S. K. S. Gupta, E. Elsharawy, and L. Schwiebert, "Towards a propagation model for wireless biomedical applications," in *IEEE ICC 2003*, vol. 3, May 2003, pp. 1993–1997.

[20] "A practical guide to the determination of human exposure to radio frequency fields. report no. 119," National Council on Radiation and Measurements, Bethseda, MD, 1993.

[21] H. H. Pennes, "Analysis of tissue and arterial blood temperature in the resting human forearm," *Journal of Applied Physiology*, vol. 1.1, pp. 93–122, 1948.

[22] D. M. Sullivan, *Electromagnetic Simulation Using the FDTD Method*. IEEE Press, 2000.

[23] Tissue dielectric properties. [Online]. Available: http://www.fcc.gov/cgi-bin/dielec.sh

[24] S. C. DeMarco, G. Lazzi, L. Wentai, J. D. Weiland, and M. S. Humayun, "Computed SAR and thermal elevation in a 0.25-mm 2-D model of the human eye and head in response to an implanted retinal stimulator - part I: Models and methods," *IEEE Tran. Antennas and Propagation*, vol. 51, no. 9, pp. 2274–2285, Sept. 2003.

[25] Q. Huang and M. Oberle, "A 0.5 mW passive telemetry IC for biomedical applications," *IEEE J. Solid-State Circuits*, vol. 33, pp. 937–946, 1998.

[26] G. Lazzi, S. C. DeMarco, L. Wentai, J. D. Weiland, and M. S. Humayun, "Computed SAR and thermal elevation in a 0.25-mm 2-D model of the human eye and head in response to an implanted retinal stimulator - part II: Results and methods," *IEEE Tran. Antennas and Propagation*, vol. 51, no. 9, p. 2286–2295, Sept. 2003.

[27] Tablecurve 3D. [Online]. Available: http://www.systat.com/

[28] Z. Michalewicz, *Genetic algorithms + data structures = evolution programs (2nd, extended ed.)*. Springer-Verlag New York, Inc., 1994.

[29] L. Davis, "Applying adaptive algorithms to epistatic domains," in *Proc. 9th Int'l Joint Conf. Artificial Intelligence*, Los Angeles, CA, 1985.